An Indoor Backpack System for 2-D and 3-D Mapping of Building Interiors

Chenglu Wen, *Member, IEEE*, Siyu Pan, Cheng Wang, *Senior Member, IEEE*, and Jonathan Li, *Senior Member, IEEE*

***Abstract*—This letter presents a backpack mapping system for creating indoor 2-D and 3-D maps of building interiors. For many applications, indoor mobile mapping provides a 3-D structure via an indoor map. Because there are significant roll and pitch motions of the indoor mobile mapping system, the need arises for a moving mobile system with 6 degrees of freedom (DOFs) (x, y, and z positions and roll, yaw, and pitch angles). First, we present a 6-DOF pose estimation algorithm by fusing 2-D laser scanner data with inertial sensor data using an extended Kalman filter-based method. The estimated 6-DOF pose is used as the initialized transformation for consecutive map alignment in 3-D map building. The 6-DOF pose gives a full 3-D estimation of the system pose and is used to accelerate the map alignment process and also align the two maps directly when there are few or no overlapping areas between the maps. Our results show that the proposed system effectively builds a consistent 2-D grid map and a 3-D point cloud map of an indoor environment.**

***Index Terms*—Indoor mobile mapping, point clouds, scan registration, 6-degree-of-freedom (DOF) localization.**

I. Introduction

THE three-dimensional mapping of building interiors can be used in applications, such as simulating disaster management, displaying virtual reality, mapping hazardous environments, etc. Traditional ways to obtain 3-D maps of building interiors mainly rely on hand drawings, reconstruction using design data, or terrestrial laser scanning. When dealing with buildings with complex internal structures, these methods are labor and time consuming. Indoor mobile mapping provides a solution to mapping an indoor environment on a mobile platform (pushcart, robot, or human) [1]–[4].

There are many ways to obtain 3-D data, for example, rotating a 2-D laser scanner [5] to achieve 3-D data, stereo vision, and time of flight cameras. Some 3-D mapping technologies have already been used in indoor search and rescue applications [6]. For traditional indoor mobile mapping systems, the localization algorithms used were based on an assumption that the system moves only in a 2-D plane. The application of the Bayesian probability model, 2-D simultaneous localization and mapping (SLAM) solutions, based on a 2-D laser scanner, has achieved great success [7]. Nowadays, many localization algorithms and mapping systems have been developed to explore in real 3-D space [8], [9].

From our previous work [10], the mobile mapping system, moving in 2-D, acquires 3-D point features that are used for building a 3-D map, which is considered as a 4-degree-of-freedom (DOF) $(x = [x_i, y_i, z_i, \phi_i])$ 3-D SLAM. Many mapping tasks, such as indoor disaster search and rescue, require the system to move in 3-D space and generate a 3-D map, which is referred to as 6-DOF (roll, yaw, and pitch angles in the XYZ plane) mapping.

In this letter, we first apply a backpack mobile mapping system to indoor non-GPS/GNSS (Global Navigation Satellite System) situations. The backpack system, carried by a person, is subject to significant roll and pitch during movement; those motions of the system create the need for 6-DOF for the pose estimation of the mapping system. We propose a pose tracking algorithm for a mobile mapping system to fuse the 2-D laser scanner and inertial sensor data for 6-DOF pose tracking by using an extended Kalman filter (EKF)-based method. The estimated 6-DOF pose is used as the initialization transformation for consecutive map alignment in creating a 3-D map. The 6-DOF pose gives a full 3-D estimation of the system pose and is used to accelerate the map alignment process and align two maps directly when there are few or no overlapping areas between the maps.

II. System Design

A. Backpack System Design

The mapping system consists of three 2-D laser scanners and one microelectromechanical-system inertial measurement unit (IMU) [see Fig. 1(a)]. A horizontally mounted laser scanner, which achieves 2-D horizontal scan profiles, is used to build a 2-D map of the building based on a particle filter-based SLAM algorithm. Simultaneously, the system provides 2-D pose information of the mapping system at each location. The backpack system's 6-DOF pose is achieved by fusing the horizontally mounted 2-D laser scanner and IMU data. Two vertically mounted laser scanners are used to create 3-D point clouds of the indoor environment. Two well-calibrated laser scanners are mounted so that each faces the side of a wall. The 2-D laser profiles acquired by these two laser scanners are registered on a coordinate system using the system's 6-DOF pose. Detailed hardware information about the system is shown in Table I.

Manuscript received December 15, 2015; revised March 1, 2016 and April 2, 2016; accepted April 21, 2016. Date of publication May 11, 2016; date of current version June 10, 2016. This work was supported by the National Science Foundation of China through Project 61401382.

C. Wen, S. Pan, and C. Wang are with the Fujian Key Laboratory of Sensing and Computing for Smart City and the School of Information Science and Engineering, Xiamen University, Xiamen 361005, China, and also with the Fujian Collaborative Innovation Center for Big Data Applications in Governments, Fuzhou 350003, China (e-mail: clwen@xmu.edu.cn; 506381813@qq.com; cwang@xmu.edu.cn).

J. Li is with the Fujian Key Laboratory of Sensing and Computing for Smart City and the School of Information Science and Engineering, Xiamen University, Xiamen 361005, China, with the Fujian Collaborative Innovation Center for Big Data Applications in Governments, Fuzhou 350003, China, and also with the GeoSTARS Lab, Department of Geography and Environmental Management, University of Waterloo, Waterloo, ON N2L 3G1, Canada (e-mail: junli@xmu.edu.cn).

Color versions of one or more of the figures in this paper are available online at http://ieeexplore.ieee.org.

Digital Object Identifier 10.1109/LGRS.2016.2558486

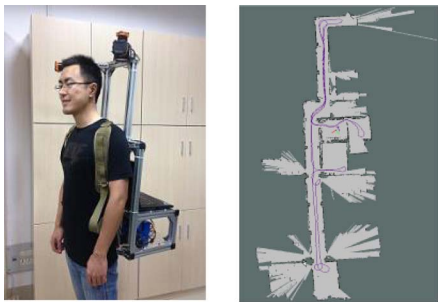

(a) (b)

Fig. 1. (a) Backpacked indoor mapping system. (b) Two-dimensional map built.

TABLE I
HARDWARE INFORMATION

Equipment	Specifications
Laser scanner	UTM-30LX, 0.1 to 10m:±30mm, 10 to 30m:±50mm Approx. 0.37kg (with cable attachment) [11]
IMU	Xsens mti-10, Gyroscopes: 450°/s, Accelerometers: 50m/s², 57x42x23.5 mm, 0.052kg [12]
Battery	lithium battery, 12V 20AH, 127x72x52 mm, 0.973kg
Processing unit	HP ENVY 15-ae125TX, 384x255x23mm, 1.9kg
Trestle	Aluminum, 5kg

B. Two-Dimensional Map Building

The mapping system uses a particle filter method, the Rao–Blackwellized particle filter (RBPF), as a 2-D SLAM solution for creating a 2-D grid map. The RBPF accurately generates potential particle distribution (weights the particles based on a probabilistic model of the odometer estimation and the scan matching considering the 2-D range data) and adaptively resamples the particles to avoid particle depletion. With 2-D laser scanner data, the 2-D SLAM process provides a 2-D map of the environment and also provides an initial pose estimation of the mapping system. These 2-D pose data are also used in 3-D scan registration [10]. An example of a 2-D map of an indoor environment that is built based on a particle filter-based 2-D SLAM algorithm using a horizontally mounted laser scanner is shown in Fig. 1(b). The red line in this figure is the 2-D trajectory of the platform.

III. 6-DOF POSE ESTIMATION-BASED MAPPING

A. EKF-Based 6-DOF Pose Estimation

We developed a 6-DOF pose estimation algorithm for system pose tracking when the system is exploring a 3-D space. The localization algorithm fuses the 2-D laser scanner and IMU data by an EKF method. To achieve a more accurate 3-D system pose, the IMU accurately measures each roll and pitch angle of the system. The estimated 6-DOF pose is used as the initialized transformation for consecutive map alignment in 3-D map building. The 6-DOF pose provides a full 3-D estimation of the system pose and is used to accelerate the map alignment process and align the two maps directly when there are few or no overlapping areas between the maps.

Next, the mapping system, consisting of a 3-axial accelerometer and a 3-axial rate gyro, equipped with inertial sensors, achieves an orientation and absolute inclination. The mapping system provides pitch (θ_i) and roll (ψ_i) data for the system, forming a 6-DOF pose. The system provides a full 6-DOF pose of a robot or platform with a combination of a 2-D laser scanner and an inertial sensor via the EKF method in 3-D space [13].

For a given time i, the system's 6-DOF pose is represented as

$$x = \left[(x_i, y_i, z_i)^T, (\phi_i, \theta_i, \psi_i)^T, (x_{vi}, y_{vi}, z_{vi})^T\right]^T \quad (1)$$

where the first component is the position; the second component is the roll, pitch, and yaw; and the third component is the instant velocity in different directions. The 6-DOF pose is written as

$$x = \left[(x_i, y_i, z_i)^T, \left[(\omega_{i1}, \omega_{i2}, \omega_{i3})^T \cdot E\right], \left[(\alpha_{i1}, \alpha_{i2}, \alpha_{i3})^T \cdot RO + G\right]\right]^T \quad (2)$$

where $(\omega_1, \omega_2, \omega_3)^T$ are angular rate and $(\alpha_1, \alpha_2, \alpha_3)^T$ are accelerations. E maps the angular rates to the derivatives of the Euler angles, RO is the direction cosine matrix mapping a vector to the navigation frame, and G is the constant gravity frame. The estimated state and covariance of the EKF integration of the IMU data with 2-D laser scanner-based SLAM are

$$\begin{aligned}(\mathrm{C}_t)^{-1} &= (1-w)C_{t-1} + wO^T M_{t-1} O \\ x_t &= C_t\left((1-w)C_{t-1}x + wO^T M_{t-1}(x_{li}, y_{li}, \psi_{li})^T\right)^{-1}\end{aligned} \quad (3)$$

where O is the observer matrix projecting the state space into 3-D space; $w \in (0, 1)$ gives the weight to update the pose according to the importance of the SLAM. The rigid transformation from 2-D laser scanner-based SLAM is $(x_{li}, y_{li}, \psi_{li})^T$, and the covariance matrix of the 2-D SLAM is M.

The EKF-based fusion method estimates the roll, pitch, and yaw values of the platform by an EKF fusion process. The 2-D pose (x, y, and orientation) from the 2-D SLAM and the localization and pose values achieved directly from the IMU are the inputs to the EKF.

B. Three-Dimensional Scan Registration Based on 6-DOF Pose

The two vertical laser scanners continuously achieve 3-D scans while the backpack mapping system is exploring an indoor environment. Each scan represents the observation of the real world from the mapping system at a certain time and location. The 3-D scan registration registers all the scans to a global coordinate system to finally create a global 3-D map. The specific steps of the multiscan registration strategy, in detail, are as follows.

First, a global coordinate system is defined when a mapping system moves to a new indoor environment. The initial position of the mapping system is set at the origin of the coordinate system, where the x-axis is the mapping system's direction of movement, the y-axis is the mapping system's left direction, and the z-axis is the direction perpendicular to the ground. During the map-building process, a 3-D map is built incrementally by referencing the global coordinate system along with an increase in observations.

The mapping system continuously obtains new 3-D scans when it explores the indoor environment. We set every five seconds' scan data as one frame. The current scan (F_{current}), indicating the current five seconds' scan data, is registered to the previous scan (F_{previous}), indicating the previous five seconds' scan data. The rigid transformation (T) between the scans is

calculated using an iterative-closest-point method [14]. T is initialized by the platform 6-DOF pose. When dealing with frame aligning, where insufficient correspondence or nonoverlapping frames exist, the iterative convergence of T is replaced by a transformation of the platform 6-DOF pose. The rigid transformation (T_{global}) between the current scan and the global coordinate system is updated by $(T_{\text{global}} = T_{\text{global}} \times T)$. In addition, the previous scan is updated by $(F_{\text{previous}} = F_{\text{current}})$ for the next registration calculation.

The current 3-D scan in the global coordinate system, $(F_{\text{current}\prime})$, is calculated by $F_{\text{current}\prime} = T_{\text{global}}(F_{\text{current}}) = (R \times F_{\text{current}} + t)$. R and t are the rotation and translation components of the transformation T_{global}. After removing the noise, $F_{\text{current}\prime}$ is added to the global 3-D map, and the global 3-D map is updated. When the mapping system ceases to search, the map is saved, and the process is terminated.

C. Closed-Loop Detection and Global Optimization

The 3-D mapping's registration error accumulates while the mapping system continuously searches an indoor environment. The 3-D map will not overlap when the mapping system returns to a location that has been visited previously, resulting in a loop closure problem. To achieve a globally consistent map, the closed-loop detection process requires the mapping system to detect the closed loop and eliminate the accumulated registration error. Because the sensors for 2-D and 3-D data acquisition are rigid in the mapping system, the 2-D and 3-D maps built are considered to be congruent for a given position. Thus, in 2-D SLAM, a closed-loop detection solution, based on a particle filter method, is equally suitable for solving closed-loop detection in 3-D mapping. Based on this idea, we apply a graph-based optimization framework for optimal mapping system pose estimation when a closed loop is detected in 2-D SLAM.

First, we continually monitor the particle filter weights in RBPF-based 2-D SLAM. The mapping system encounters a closed loop when the particle weight is smaller than a setting threshold value. At this point, the particle filter commences to resample and reset the weights of all the particles, correct the mapping system pose, and update the 2-D map [9]. Then, we adopt a graph theory-based method to eliminate cumulative error and build a globally consistent map. We build a graph structure of the global 3-D map based on the general-graph-optimization framework [15]. In the graph structure, the system poses and registration errors between scans are represented as nodes and edges, respectively. The graph structure's error equation is minimized using the Levenberg–Marquardt iterative algorithm, and the maximum likelihood system poses are estimated. Then, the global 3-D map is updated using the transformation matrix converted by the estimated system poses.

IV. Experiments and Results

A. Three-Dimensional Mapping Result

An example of a 3-D point cloud map with a closed loop built by our system is given in Fig. 2(a), an example of a 3-D point cloud built for a larger area with multiple rooms is given in Fig. 2(b), an a multifloor indoor scene result is given in Fig. 2(c). The corresponding images of the real scenes are shown in Fig. 2(d)–(f), respectively. The results show that our system achieves a robust map-building performance on loop closure and also maintains relatively good consistency between the 2-D and 3-D maps for large indoor scenes and multifloors.

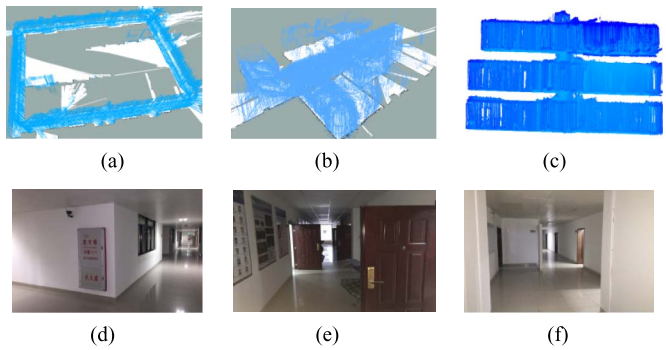

Fig. 2. Examples of 3-D map built by our system. (a) Closed-loop corridor. (b) Another indoor scene result. (c) Multifloor indoor scene result. (d) Correspondent real scene image of (a). (e) Correspondent real scene image of (b). (f) Correspondent real scene image of (c).

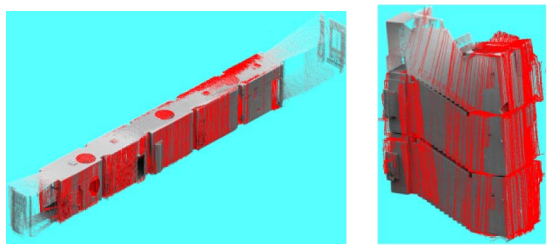

Fig. 3. Point clouds acquired by our system and VZ-1000. Red scans are our data; gray scans are VZ-1000 data. (a) Corridor result. (b) Stairs result.

B. Three-Dimensional Mapping Accuracy Compared With High-Precision Mapping System

We compared our mapping results with a high-precision mapping system on the 3-D point clouds of an indoor scene. We used the high-precision 3-D mapping system, RIEGL VZ-1000 3-D laser scanner, to provide ground truth for comparing the 3-D map that was built. The RIEGL VZ-1000 laser scanner provides a measurement range of more than 1400 m, a measurement rate up to 122 000 measurements per second, and a scanning accuracy of approximately 5 mm (100 m from the single point of scanning) [16].

We first directly compared our system's 3-D point cloud with the VZ-1000's 3-D point cloud by points. Fig. 3 shows the registered point clouds acquired by our system and the VZ-1000 system. Red scans are our data; gray scans are VZ-1000 data. The length of the corridor selected for collecting data is about 30 m. The human operator's walking speed was about 0.5 m/s. It took approximately 1 min to complete collecting the data for the backpack system.

We selected eight pillars in the corridor as a reference. Then, we selected the columns at the exact lines where the columns and floor intersect. Four intersecting lines of each column were selected and located manually in the 3-D point cloud. For comparison, we calculated the average distance error on two corresponding lines of two neighbored pillars. The distances measured between the pillars on our system's 3-D point cloud and the VZ-1000's 3-D point cloud are given in Table II. The

TABLE II
PERFORMANCE COMPARISON BETWEEN BACKPACK MAPPING SYSTEM AND HIGH-PRECISION LASER SCANNER SYSTEM

Distance(m)	Distance by VZ-1000	Distance by 3-D data
Pillar 1~ Pillar 2	6.01511	5.97702
Pillar 3~ Pillar 4	6.02130	6.12213
Pillar 5~ Pillar 6	6.00154	6.08810
Pillar 7~ Pillar 8	6.03200	5.98302
Average error	0	1.14%

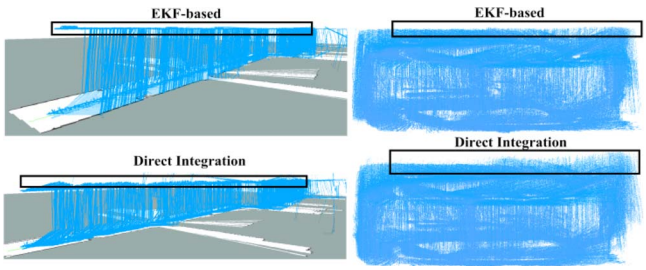

Fig. 4. Comparison of 3-D scans acquired between the EKF-based and the direct-integration method: (a) Corridor scene and (b) room scene.

results of the VZ-1000 are considered the references, in which the errors are set to zero. The average location error of the 3-D map built by our system is 1.14%.

We also calculated the vertical and planimetric precisions of the collected point clouds by our system. In Fig. 3(a), assuming that the corridor within a small local area is flat, the floor data within a small rectangle are selected to calculate the vertical precision. Local precision is determined by evaluating the residuals following a least square of the points to the plane. The average standard deviation is 2.26 cm. Similarly, the data on a vertical wall are selected to assess the planimetric precision of the collected point clouds. The average standard deviation is 14.83 cm.

C. Scan Registration Based on 6-DOF Pose

Second, using different methods to register 3-D scans, we compared the accuracies of different methods with added IMU data in the 3-D map-building process. The direct-integration and the EKF-based fusion method are used to form a 6-DOF pose of the platform. The direct-integration method acquires the platform's pose (roll, pitch, and yaw) values directly from the IMU. Over time, the cumulative error in the pose achieved directly from the IMU will become large. Two examples of 3-D point clouds acquired with the Kalman filter-based and the direct-integration method are shown in Fig. 4. The ceiling and floor areas highlighted by the blocks in black show that the Kalman filter-based method to establish a 3-D map has better performance than the direct-integration method.

To further compare the 3-D point cloud data acquired using the Kalman filter-based method with the direct-integration method, we compared two results via the planes extracted. We extracted lines and planes from the 3-D point cloud obtained by our system and compared them with the values manually obtained from the VZ-1000 results (as references) and the positional relationships (parallel vertical, etc.) between each plane using the method proposed in our previous work [17]. As shown in Fig. 5, lines and planes are extracted for two indoor scenes.

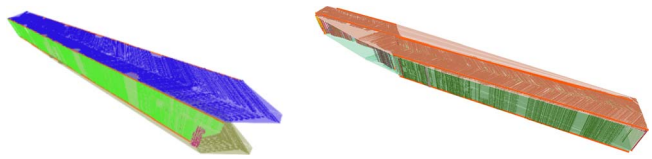

Fig. 5. Line and plane extraction results. (a) Straight corridor. (b) Corridor with a corner.

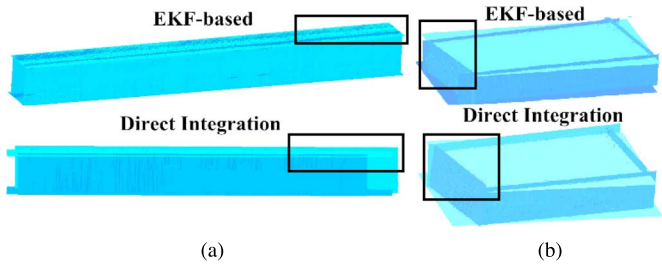

Fig. 6. Comparison of planes extracted between the EKF-based and the direct-integration method: (a) Corridor scene and (b) room scene.

TABLE III
PERFORMANCE COMPARISON BETWEEN THE KALMAN FILTER-BASED AND THE DIRECT-INTEGRATION METHOD IN PLANE EXTRACTION

Scenes	Parameters	Reference (VZ-1000)	EKF -based	Direct integration
Corridor	Point number	/	834781	639121
	Deviation: angle	0°	1.07°	6.36°
	Deviation: distance	0m	0.03m	0.18m
	Time cost	/	15.3s	11.8s
Room	Point number	/	3032093	2892666
	Deviation: angle	0°	3.18°	7.56°
	Deviation: distance	0m	0.09m	0.21m
	Time cost	/	62.3s	58.5s

Red lines represent the extracted framework lines, including intersecting lines among the wall, floor and ceiling, doors, etc. Colors, other than red, represent different extracted planes.

Fig. 6 shows the plane extraction results and a comparison of the plane obtained by using the EKF-based fusion method with the plane obtained by using the direct-integration method. In the plane extraction results, the EKF-based method exhibits better performance than the direct-integration method. As shown in Fig. 6, the extracted plane using direct integration has many errors, such as those beyond the ceiling, walls, and floor. Point clouds, using the EKF-based fusion method, have fewer errors in the z-axis than point clouds using direct integration.

To quantitatively evaluate the two results, we counted and recorded the total number of points across the two scenes in plane extraction and the time spent by the EKF-based fusion method and direct-integration method. We measured the average errors in distance and angle from an extracted plane and the floor plane extracted from the 2-D map (see Table III). In the corridor scene, the EKF-based method has a 0.03-m average offset in the z-axis; the direct-integration method has a 0.18-m average offset. The EKF-based method has a 1.07° average angle offset; the direct-integration method has a 6.36° average angle offset. The error using the EKF-based fusion method is much lower than the error using direct integration in the plane extraction. The time cost of the EKF-based method is 15.3 s; the time cost of the direct-integration method is 11.8 s. In the room scene, the EKF-based method has a 0.09-m average offset in the z-axis; the direct-integration method has a 0.21-m

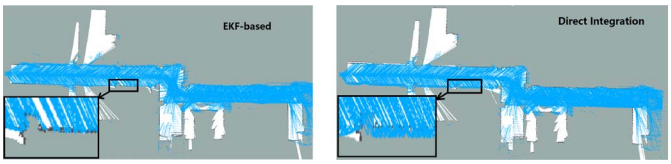

(a) (b)

Fig. 7. Consistency of 2-D and 3-D maps built. (a) Result by EKF-based fusion method. (b) Result by direct-integration method.

TABLE IV
RESULT COMPARISON BETWEEN 2-D MAP AND 2-D DATA PROJECTED FROM 3-D

Distance(m)	2-D map	2-D data projected from 3-D
Pillar 1~ Pillar 2	6.08200	5.98902
Pillar 3~ Pillar 4	6.08135	6.11731
Pillar 5~ Pillar 6	5.98923	6.09221
Pillar 7~ Pillar 8	6.08151	6.00982
Average error	0	1.25%

average offset. The EKF-based method has a 3.18° average angle offset; the direct-integration method has a 7.56° average angle offset. The time cost of the EKF-based method is 62.3 s; the time cost of the direct-integration method is 58.5 s. To remove the erroneous points, we filtered the data for both of the acquired point clouds. The EKF-based method acquired more accurate 3-D point clouds, and fewer points were filtered. The direct integration-based method acquired less accurate 3-D point clouds, and more points were filtered.

D. Consistency of 2-D and 3-D Maps

Examples of 2-D and 3-D maps built by the EKF-based and direct-integration methods are given in Fig. 7. The EKF-based method generally exhibits better consistency between the 2-D and 3-D maps, particularly in the corners and small spaces. The possible reason is that, compared to the open and flat areas, a larger pose change is acquired when the platform explores the corners and small space areas.

To verify the consistency of the 2-D and 3-D maps built by our system, we compared the difference to establish the 3-D map projected to a 2-D plane with the 2-D grid map. We used the 2-D grid map built by 2-D SLAM as a reference to compare the pillar contrasting with the 3-D map and a 2-D grid map. First, we built a 3-D point cloud map and projected it onto a 2-D map, ignoring z-axis height changes. Next, we selected the columns at the exact lines where the columns and floor intersect. Every column has two lines selected and located in the 2-D map projected by a 3-D point cloud. Then, we calculated the average distance error between the 3-D point clouds and projected it onto 2-D and 2-D grid maps. The results of the comparison between the distance in 2-D map and 2-D data projected from 3-D are shown in Table IV. The average error between the 3-D point cloud and 2-D grid map is 1.25%.

V. CONCLUSION

This letter has presented a backpack mobile mapping system that is designed mainly for non-GNSS/GPS indoor use. By introducing 6-DOF localization, the system provides 2-D and 3-D maps for an indoor environment. In the experiments, we discovered that the proposed EKF-based method fusing 2-D laser scanning and IMU data greatly reduces the error when the system is moving. For 3-D point clouds, using IMU results in the building of a more accurate 3-D map.

REFERENCES

[1] M. Fallon, H. Johannsson, J. Brookshire, S. Teller, and J. Leonard, "Sensor fusion for flexible human-portable building-scale mapping," in *Proc. IEEE/RSJ Int. Conf. IROS*, 2012, pp. 4405–4412.
[2] N. Corso and A. Zakhor, "Indoor localization algorithms for an ambulatory human operated 3-D mobile mapping system," *Remote Sens.*, vol. 5, no. 12, pp. 6611–6646, Oct. 2013.
[3] P. Henry, M. Krainin, E. Herbst, X. Ren, and D. Fox, "RGB-D mapping: Using kinect-style depth cameras for dense 3-D modeling of indoor environments," *Int. J. Robot. Res.*, vol. 31, no. 5, pp. 647–663, 2012.
[4] M. Bosse, R. Zlot, and P. Flick, "Zebedee, design of a spring-mounter 3-D range sensor with application to mobile mapping," *IEEE Trans. Robot.*, vol. 28, no. 5, pp. 1104–1119, Oct. 2012.
[5] J. Zhang and S. Singh, "LOAM: Lidar odometry and mapping in real-time," in *Proc. Robot., Sci. Syst. Conf.*, Jul. 2014, pp. 1–9.
[6] L. Ellekilde, S. Huang, V. Miróand, and G. Dissanayake, "Dense 3-D map structure for indoor search and rescue," *J. Field Robot.*, vol. 24, no. 1/2, pp. 71–89, 2007.
[7] S. Thrün *et al.*, "Simultaneous localization and mapping with sparse extended information filters," *Int. J. Robot. Res.*, vol. 23, no. 7/8, pp. 693–716, 2004.
[8] B. K. Kim, "Indoor localization and point cloud generation for building interior modeling," in *Proc. 22nd IEEE Int. Symp. Robot. Human Interactive Commun.*, Gyeongju, South Korea, 2013, pp. 186–191.
[9] T. Liu *et al.*, "Indoor localization and visualization using a human-operated backpack system," in *Proc. Int. Conf. IPIN*, Zurich, Switzerland, 2010, pp. 1–10.
[10] C. Wen, L. Qin, Q. Zhu, C. Wang, and J. Li, "Three-dimensional indoor mapping with fusion of two-dimensional laser scanner and RGB-D camera data," *IEEE Geosci. Remote Sens. Lett.*, vol. 11, no. 4, pp. 843–847, Apr. 2014.
[11] [Online]. Available: http://www.hokuyo-aut.jp/02sensor/07scanner/utm_30lx.html
[12] [Online]. Available: https://www.xsens.com/products/mti-10-series/
[13] S. Kohlbrecher, S. Von, J. Meyer, and U. Klingauf, "A flexible and scalable slam system with full 3-D motion estimation," in *Proc. IEEE Int. SSRR.*, 2011, pp. 155–160.
[14] S. Rusinkiewicz and M. Levoy, "Efficient variants of the ICP algorithm," in *Proc. 3rd Int. Conf. 3D Digit. Imag. Model.*, 2001, p. 145.
[15] R. Kuemmerle, G. Grisetti, and H. S. trasdat, "g2o: A general framework for graph optimization," in *Proc. IEEE Conf. Robot. Autom.*, Shanghai, China, 2011, pp. 3607–3613.
[16] [Online]. Available: http://www.riegl.com/uploads/tx_pxpriegldownloads/DataSheet_VZ-1000_2015-03-24.pdf
[17] Y. Lin *et al.*, "Line segment extraction for large scale unorganized point clouds," *ISPRS J. Photogram. Remote Sens.*, vol. 102, pp. 172–183, 2015.